

Optimization strategies to obtain smooth gait transitions through biologically plausible central pattern generators

V. Baruzzi , M. Lodi , and M. Storaice *

Department of Electrical, Electronics and Telecommunication Engineering and Naval Architecture, University of Genoa, 16145 Genoa, Italy



(Received 11 July 2023; accepted 7 December 2023; published 22 January 2024)

Central pattern generators are small networks that contribute to generating animal locomotion. The models used to study gait generation and gait transition mechanisms often require biologically accurate neuron and synapse models, with high dimensionality and complex dynamics. Tuning the parameters of these models to elicit network dynamics compatible with gait features is not a trivial task, due to the impossibility of inferring *a priori* the effects of each parameter on the nonlinear system's emergent dynamics. In this paper we explore the use of global optimization strategies for parameter optimization in multigait central pattern generator (CPG) models with complex cell dynamics and minimal topology. We first consider an existing quadruped CPG model as a test bed for the objective function formulation, then proceed to optimize the parameters of a newly proposed multigait, interlimb hexapod CPG model. We successfully obtain hexapod gaits and prompt gait transitions by varying only control currents, while all CPG parameters, once optimized, are kept fixed. This mechanism of gait transitions is compatible with short-term synaptic plasticity.

DOI: [10.1103/PhysRevE.109.014404](https://doi.org/10.1103/PhysRevE.109.014404)

I. INTRODUCTION

Central pattern generators (CPGs) are relatively small neural circuits that play a fundamental role in multiphase animal locomotion [1,2]. They can autonomously produce rhythmic patterns of neural activity, independently from the presence of sensory feedback or inputs from higher areas [3]. Sensory feedback can, however, adapt and fine-tune the activity of the CPG to the environment [4], while hierarchically higher areas can, for example, prompt transitions between gaits [5–7].

Numerous studies have applied experimental and theoretical approaches to unravel the structure and function of animal CPGs and their interactions with other key structures governing animal locomotion [8–10], leading to the development of many biologically informed mathematical models [11–14] which aim to retain sufficient detail to pursue the investigation of biophysical CPG properties, but also reduce complexity to allow meaningful interpretation of the results. Simplified CPG-inspired oscillator networks are also of great interest in the field of bioinspired robotics, constituting the basis for efficient, robust, and distributed locomotion control systems [15,16].

The CPG capability of generating rhythmic patterns results from the interplay of the topology of the neural network and the dynamics of both neurons and synapses.

In this work, we maintain complex, high-dimensional neuron models and use dynamic synapse models, without compromising biological accuracy, with the goal of modeling biologically plausible gait transition mechanisms. On the other hand, we represent the multigait interlimb CPGs

employing minimalist topologies, with few network nodes, hereby called cells.

As stated above, while CPGs can operate independently, transitions between gaits are modulated by the action of higher areas. In CPG models, a single gait is achieved by keeping the connectivity fixed; to generate multiple gaits, usually the control mechanism of the brainstem is mimicked by adjusting the synaptic conductances. Biologically, however, changes in conductance values result from long-term synaptic plasticity, making them unsuitable to model quick gait switches. For this reason, in our previous work [17,18] and in the present paper, we implement gait transitions by modifying the input control currents received by the CPG cells.

We propose a method to set the many model parameters by defining a proper objective function that drives the optimization to a parameter set that elicits the desired emergent dynamics of the CPG network in terms of gait features. The use of global optimization strategies for CPG parameter setting is explored, first, by using the quadruped CPG model proposed in [18] as a test bed, improving the accuracy in reproducing the target quadruped gaits. Second, we optimize the parameters of an interlimb hexapod CPG model with a minimalist topology, but accurate neuron and synapse models, with the goal of reproducing the three main hexapod gaits and biologically plausible gait transitions. We successfully obtain a parameter set that allows reproducing the three target gaits and smooth gait transitions by modifying only the input control currents.

II. CPG PRIMARY ELEMENTS: CELLS AND SYNAPSES

We model the CPG cells with the thalamic reticular burster [19,20] within the Hodgkin-Huxley (HH) framework (see Appendix A for details). The dynamics of the membrane

*Corresponding author: marco.storaice@unige.it

potential V_i and of the voltage-dependent state variables $\mathbf{y}_i \in \mathbb{R}^6$ (representing intracellular calcium concentration and gating variables) are governed by HH-type ODEs:

$$\frac{d}{dt} \begin{bmatrix} V_i \\ \mathbf{y}_i \end{bmatrix} = \begin{bmatrix} -\sum_k I_k + I_c + I_i^{syn} \\ \mathbf{f}(V_i, \mathbf{y}_i) \end{bmatrix}, \quad (1)$$

where the sum $\sum_k I_k$ includes the intracellular ionic currents, and the current I_c , modeling the modulation from higher areas, is used as the control parameter; the components of $\mathbf{f}(V_i, \mathbf{y}_i)$ modeling gating variables' dynamics are logistic or sigmoidal functions. This model produces bursting activity for $I_c \in [-0.43, 0.13] \frac{\mu A}{cm^2}$ [17]. The term I_i^{syn} groups the incoming synaptic currents,

$$I_i^{syn} = \sum_{j=1}^N \sum_S g_{ij}^S [E^S - V_i(t)] s_j^S, \quad (2)$$

where S denotes the synapse type, E^S represents the reversal potential, $0 \leq s_j^S(V_i, t) \leq 1$ describes the neurotransmitter release rate of the synapse, and g_{ij}^S is the maximal synaptic conductance or weight.

Synapses are either modeled using the fast threshold modulation (FTM) approach [21,22], $s_j^S = f_\infty^S(V_j)$ or described by a first-order kinetic model [21,23–25],

$$\begin{aligned} \frac{ds_j^S}{dt} &= \alpha (1 - s_j^S) f_\infty^S(V_j) - \beta s_j^S, \\ f_\infty^S &= \frac{1}{1 + e^{-\nu(V_j - \theta^S)}}, \end{aligned} \quad (3)$$

where θ^S is the synaptic threshold, and α and β are coefficients determining the exponential rise and decay rates, respectively: the greater the α (β) values, the faster the rise (decay) rates of s_j^S after the presynaptic voltage V_j goes over (under) θ^S .

III. FITTING STRATEGY

In our previous works [14,18] we proposed a custom optimization strategy for the parameter setting of a quadruped CPG: the strategy hierarchically subdivides the problem into consecutive simpler steps, considering subnetwork units separately. Although efficient in terms of computational cost, and effective in clarifying the role of each unit and synapse, this optimization strategy does not capture the interplay of all model elements, leaving the dynamics of the final CPG network to be verified *a posteriori*.

In this paper, we propose a method to define an objective function for setting the parameters of biologically plausible CPGs, which can be used for any number of legs. The objective function is defined with the goal of obtaining a CPG model with fixed topology and synaptic conductances, able to exhibit multiple gaits and smooth gait transitions when varying the control currents. In particular, we explore the use of global optimization strategies to set the model parameters that play a crucial role in determining the emergent dynamics of the CPG network, namely, synaptic conductances and control currents.

TABLE I. Target features of quadruped (mouse) gaits [29,30], in terms of frequency (f), duty cycle (d), and phase lags (Δ_{1j}).

Gait	f [Hz]	d	Δ_{12}	Δ_{13}	Δ_{14}
Walk (W)	[2 4]	<0.4	0.5	0.75	0.25
Trot (T)	[4 9]	[0.4 0.51]	0.5	0	0.5
Bound (B)	[10 12]	>0.51	0	0.5	0.5

A. Objective function

Different animal gaits are characterized by specific phase differences between limbs, and by features such as ranges of frequency and duty cycle values (see, for example, Table I and Fig. 5). When designing a multigait CPG with biologically accurate neuron and synapse models, what matters is that the activity pattern of the CPG cells matches the characteristic features of each gait. For this reason, we are interested in imposing only the high-level features of the emergent network dynamics related to each gait. In other words, we don't need the individual CPG neurons to retrace point-by-point target membrane potentials: we are interested only in obtaining a pattern of alternating bursting activity with given phase differences, frequency, and duty cycle. Following this principle, the only parameters included in the optimization process are synaptic conductances and control currents, fixing all other parameters to biologically plausible values (as detailed in Appendix A). In this paper we consider the following:

- (1) n_F target features, indicating the feature type with the index k
- (2) n_G target gaits, with \mathcal{G} indicating the gait type
- (3) A number N of legs (corresponding to N CPG cells)
- (4) A set of CPG parameters x to be optimized.

It is evident that the problem of tuning the parameters of a CPG model so that it can successfully reproduce the target gaits cannot be codified in an objective function that doesn't require the system's simulation to be calculated. The objective function can, however, be defined by comparing the n_F target features $P_{\mathcal{G},k}^*$ characterizing each one of the n_G gaits (where k identifies phase lags, frequency ranges, or duty cycle ranges) with the values of such features $P_{\mathcal{G},k}$ obtained by simulating the CPG with a certain parameter set x , as summarized in Fig. 1. In particular, for a candidate solution x , the objective function is defined as follows:

$$\epsilon(x) = \sum_{k=1}^{n_F} W_k \sum_{\mathcal{G}=1}^{n_G} \frac{1}{n_G} \mathcal{F}_k(P_{\mathcal{G},k}^*, P_{\mathcal{G},k}), \quad (4)$$

where W_k weighs the contribution of the k th gait feature to the objective function.

At each objective function evaluation, the CPG is simulated for n_G values of the control current I_c , chosen within the bursting interval so that they are compatible with the frequency and duty cycle characteristics of the desired gaits, as explained in [18]. To ensure that transitions between gaits are successful as well, each gait is simulated for initial conditions close to the phase lags of adjacent gaits. After each simulation, the membrane potentials V_i of the CPG cells at steady state are considered. Swing and stance phases are determined by thresholding the membrane potentials at a voltage level V_{th} ;

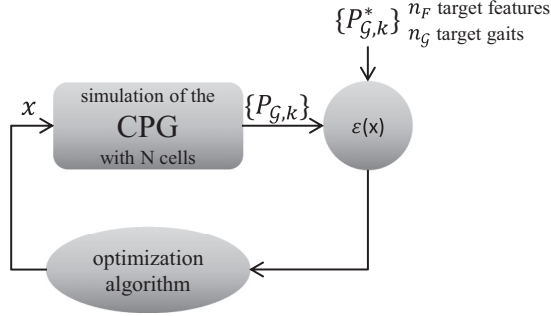


FIG. 1. The CPG model is simulated for a parameter set x , obtaining the feature values $P_{G,k}$ for n_F target features and n_G target gaits. The obtained values are compared to the reference $P_{G,k}^*$ values to calculate the objective function $\epsilon(x)$, according to which the optimization algorithm updates x .

if any cell exhibits dynamics different from regular bursting the current parameter set x is discarded by assigning an arbitrarily large value to the objective function, and the current objective function evaluation stops without performing simulations for the remaining I_c values. Otherwise, each term $\mathcal{F}_k(P_{G,k}^*, P_{G,k})$ is calculated. If k refers to phase lags, then the mean squared difference between each phase lag Δ_{1j} ($j = 2, \dots, N$) extracted from each simulation (as explained in [17]) and its target value Δ_{1j}^* is calculated:

$$\mathcal{F}_k(P_{G,k}^*, P_{G,k}) = \frac{1}{N-1} \sqrt{\sum_{j=2}^N [\text{mod}1(\Delta_{1j} - \Delta_{1j}^*)]^2}. \quad (5)$$

If k refers to frequency or duty cycle, then $\mathcal{F}_k(P_{G,k}^*, P_{G,k})$ is null if $P_{G,k}$ falls within its target range, otherwise

$$\mathcal{F}_k(P_{G,k}^*, P_{G,k}) = \frac{|P_{G,k}^* - P_{G,k}|}{P_G}, \quad (6)$$

where $P_{G,k}^*$ is the boundary of the target range nearest to $P_{G,k}$.

The obtained objective function is thus discontinuous, non-differentiable, and highly nonlinear. Derivative-free global optimization strategies that are suitable to solve this problem are based on particle swarm [26] and genetic algorithms [27]. Another aspect to consider is the high computational burden of the objective function evaluation, which requires multiple simulations of the CPG model. For this reason, surrogate optimization [28] is another suitable optimization technique, since it allows carrying out the optimization process using a smaller number of function evaluations.

IV. PRELIMINARY TESTING: RESULTS ON THE QUADRUPED CPG

We use the quadruped CPG model and its parameter set found with the custom strategy (CS) proposed in our previous work [18] as a preliminary test of the global optimization approach, with the double advantage of exploiting the *a priori* knowledge on the parameter set and, at the same time, validating the previously proposed custom strategy. In this case, the chosen target gaits are walk (W), trot (T), and bound (B) of the mouse (modeled in our previous work [18]), characterized by the phase lags, frequency, and duty cycle listed in Table I. The

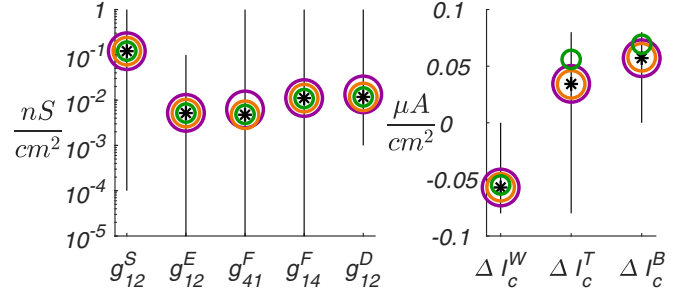


FIG. 2. Parameter sets x found by the CS (black stars), the PS optimization (orange circles), the GA optimization (green circles), and the SO algorithm (purple circles). The black vertical lines indicate the range between the lower and the upper bounds constraining the explorable parameter space.

parameter set x includes all synaptic conductances and the difference between the control currents driving the fore and hind cells for each gait \mathcal{G} : $x = \{g_{12}^S, g_{12}^E, g_{41}^F, g_{14}^F, g_{12}^D, \Delta I_c^W, \Delta I_c^T, \Delta I_c^B\}$ (see Appendix B for details on synaptic conductance notation). Taking into account the symmetries of the CPG model, we set $g_{21}^S = g_{34}^S = g_{43}^S = g_{12}^S$, $g_{21}^E = g_{34}^E = g_{43}^E = g_{12}^E$, $g_{32}^F = g_{41}^F$, and $g_{23}^F = g_{14}^F$. All other parameters were set as in Appendix B of [18].

The objective function calculation includes all features listed in Table I, with $W_k = 1$ for phase lags and $W_k = 0.02$ for frequency and duty cycle. These weights have been heuristically chosen to prioritize the generation of correct phase lags. All CPG simulations were performed using the toolbox CEPAGE [31]. The minimization of the objective function was performed using the Matlab functions *particleswarm*, *ga*, and *surrogateopt*, which implement particle swarm (PS) optimization, genetic algorithm (GA) optimization, and surrogate optimization (SO), respectively. All functions were initialized with the default options, including the number of instances of the candidate parameter set, and the explorable parameter space was constrained by imposing lower and upper bounds for each parameter in x . These bounds were chosen in accordance with the goal of obtaining regular rhythmic CPG activity. Only one instance x_0^* of the initial candidate parameter set was assigned the values obtained through the custom optimization strategy defined in [18]. The remaining instances, i.e., 79 particle positions for PS, 199 individuals for GA, and 19 sample points' coordinates for SO, were set randomly within the bounds.

All three algorithms found parameter sets x different from the instance x_0^* encoded as one of the initial candidates, indicating that all algorithms evolved beyond their initial state. As such, all algorithms reached values of the objective function $\epsilon(x)$ lower than $\epsilon(x_0^*)$, with the GA-based optimization reaching the lowest value. This result is a first confirmation of the effectiveness of the proposed optimization method in setting the multigait CPG parameters, regardless of the global optimization algorithm employed. At the same time, the solutions found by the global optimization algorithms did not drift far from x_0^* , as illustrated in Fig. 2, despite the multistart strategy adopted by these algorithms. We remark that x_0^* was only one of the many initial seeds, as stated above. This suggests that

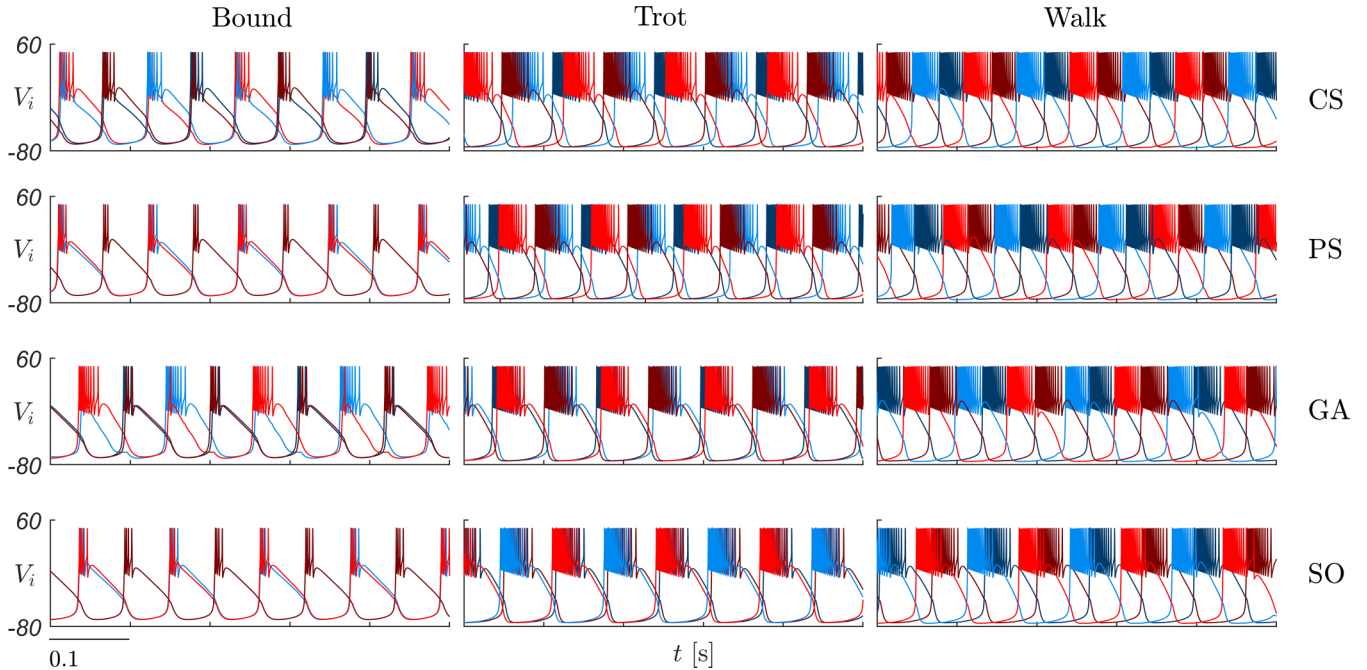


FIG. 3. Gaits obtained by simulating the quadruped CPG from [18] (see also Appendix B) with the parameter sets x found by, from top to bottom, the CS, the PS optimization, the GA optimization, and the SO algorithm. Bound was obtained for $I_c^B = -0.4243 \frac{\mu A}{cm^2}$, trot for $I_c^T = -0.0300 \frac{\mu A}{cm^2}$, and walk for $I_c^W = 0.1243 \frac{\mu A}{cm^2}$. Color coding as in Fig. 12 in Appendix B.

there are no other regions of the parameter space, distinct from the one identified by the custom optimization strategy, where the gaits are correctly reproduced, validating the effectiveness of the custom strategy. Figure 3 shows the impact of the refinement operated by the global optimization algorithms on the obtained gaits. The results for each gait are quite similar for the four considered optimization strategies (as evidenced also by the similar objective function values in Table II), and in accordance with the desired features. This suggests that, even if there is only one point minimizing the objective function, there is a non-null subspace of the parameter space corresponding to generated gaits with the desired features. This, in turn, suggests that the proposed method (CPG structure plus objective function) provides robust results.

The better outcomes of the global optimization algorithms come at the cost of a significantly higher computational load. Objective function values $\epsilon(x)$ and computing times for all algorithms are summarized in Table II. We remark that these values refer to the specific runs, and just give a general idea of the different orders of magnitude. Even when maintaining all other conditions unaltered, both the run time and the performance of the global optimization algorithms can be impacted

TABLE II. Objective function values $\epsilon(x)$ and computing times for all algorithms: custom strategy CS, particle swarm PS, genetic algorithm GA, surrogate optimization SO. T_{CS} is used as the unit for running time and corresponds to 9 hours and 38 minutes on an Intel® Xenon® CPU E5-1620 v2 at 3.70 GHz \times 8.

	CS	PS	GA	SO
$\epsilon(x)$	0.0226	0.0199	0.0119	0.0175
Running time	T_{CS}	$3.53 T_{CS}$	$24.5 T_{CS}$	$7.61 T_{CS}$

by the initialization of the particles' positions, population individuals, or points' coordinates, and likely worsened if the instance x_0^* of the initial candidate parameter set is not known *a priori*. However, the high computational cost prevents a systematic analysis over multiple runs.

V. RESULTS ON THE HEXAPOD CPG

A. Hexapod CPG model

We model the interlimb hexapod CPG according to a minimalistic topology [11,32]: one cell controlling each limb, symmetric reciprocal inhibitory connections between pairs of contralateral cells, and asymmetric reciprocal inhibitory connections between adjacent ipsilateral cells. The CPG network is shown in Fig. 4, where the cells are named according to

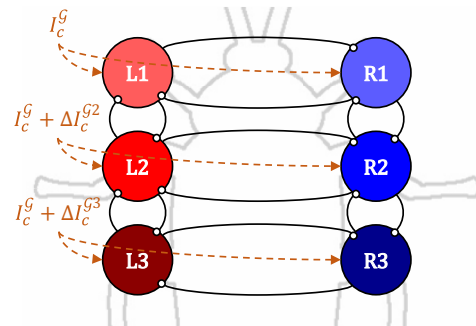


FIG. 4. Schematic of the interlimb hexapod CPG: limbs are denoted following Wilson's convention [33], and the corresponding CPG cells are named accordingly. The cell color coding established by this figure is consistent throughout the paper.

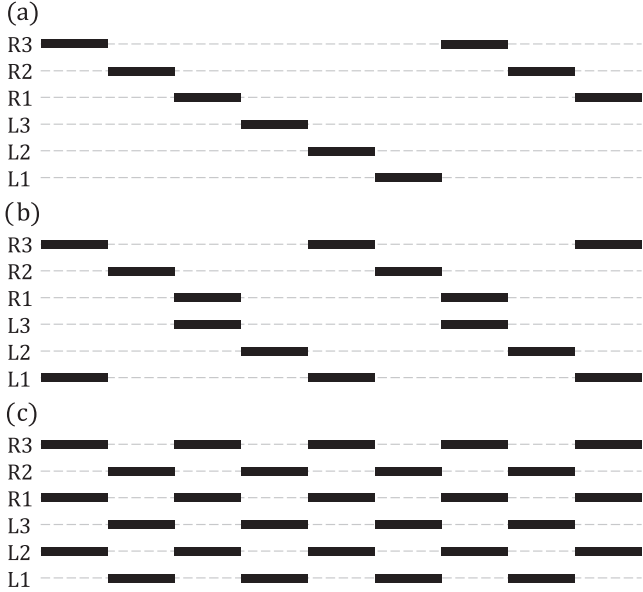


FIG. 5. Representation of three hexapod gaits: black bars indicate the swing phases, and blank spaces represent the stance phases of each leg for the (a) wave, (b) ripple, and (c) tripod gaits.

the corresponding limbs following Wilson’s convention [33]: L indicates left limbs, R indicates right limbs, and ipsilateral limbs are numbered from front to back.

All synapses are represented using the first-order kinetic model.

B. Hexapod gaits

According to Wilson’s system [33], locomotor gaits in insects comply with two central principles:

(1) Waves of forward leg movements run from posterior to anterior, and no leg moves forward until the one behind is placed in a supporting position.

(2) Contralateral legs of the same segment are always in antiphase.

These simple rules account for the vast majority of gaits observed in hexapods, with the exception of a few insect species. We focus in particular on three common gaits exhibited at slow, medium, and high speed, commonly referred to as wave (W), ripple (R), and tripod (T), summarized in Fig. 5.¹ These gaits are also compliant with the additional rules in Wilson’s system [33]:

(3) The duration of the swing phase remains constant among gaits.

(4) The frequency varies among gaits, so consequently the stance phase decreases (i.e., the duty cycle increases) as frequency increases.

(5) The intervals between adjacent ipsilateral legs are constant among gaits.

¹We remark that, despite using coinciding letters, here we are considering different gaits than in the quadruped CPG.

TABLE III. Objective function values $\epsilon(x)$ and number of function evaluations for the three global optimization algorithms (particle swarm PS, genetic algorithm GA + pattern search Psearch, surrogate optimization SO).

	PS	GA (+Psearch)	SO
$\epsilon(x)$	0.0382	0.1227 (0.1206)	0.1184
Function evaluations	11 200	18 070 (+1029)	7255

C. Results of the parameter optimization

The parameter set x includes all synaptic conductances and the differences between the control currents driving the fore and mid cells (ΔI_c^{G2}) and the fore and hind cells (ΔI_c^{G3}) for each gait \mathcal{G} : $x = \{g_{L1R1}, g_{L1L2}, g_{L2L1}, g_{L2L3}, g_{L3L2}, \Delta I_c^{W2}, \Delta I_c^{W3}, \Delta I_c^{R2}, \Delta I_c^{R3}, \Delta I_c^{T2}, \Delta I_c^{T3}\}$. Taking into account the symmetries of the CPG model, we set $g_{L1R1} = g_{R1L1} = g_{L2R2} = g_{R2L2} = g_{L3R3} = g_{R3L3}$, $g_{L1L2} = g_{R1R2}$, $g_{L2L1} = g_{R2R1}$, $g_{L2L3} = g_{R2R3}$, and $g_{L3L2} = g_{R3R2}$. In this case, the objective function is computed considering only the phase lags, since there is a large variability in frequency and duty cycle ranges exhibited by different species [34]. We instead choose to verify adherence of the obtained gaits to Wilson’s system *a posteriori*. All CPG simulations were performed using the toolbox CEPAGE [31].

Again, we test all three global optimization algorithms on the minimization of the function, this time without encoding any *a priori* knowledge in the initial state. All algorithms were initialized with their default options and the explorable parameter space was constrained by imposing lower and upper bounds for each parameter in x , allowing ranges that produce a biologically plausible behavior of the CPG model. The initial state of all algorithms (i.e., initial instances of x) was initialized randomly within the bounds.

Table III lists the objective function values and the number of function evaluations for the three algorithms. Since the genetic algorithm reached the worst objective function value, the result was further refined by employing the local derivative-free optimization strategy implemented by the *patternsearch* Matlab’s function. The particle swarm optimization reached the best result, with both the lowest value of the cost function $\epsilon(x)$ and the fewest function evaluations.

The parameter sets identified with particle swarm optimization and surrogate optimization produced stable ripple, tripod, and wave gaits, while the parameter set found by the genetic algorithm yielded a wave gait with less consistent phase lags over time. To overcome this problem, the GA-based optimization was repeated focusing only on the wave gait and simulating the CPG for a longer time interval at each objective function calculation. In this case, to reduce the computational burden, all parameters were fixed to the previously found values, with the exception of $x = \{I_c^W, \Delta I_c^{W2}, \Delta I_c^{W3}\}$. The final parameter sets found with the different algorithms are shown in Fig. 6.

Despite some parameters having significantly different values (namely, g_{L1L2} and g_{L2L3}), all parameter sets give rise to clearly recognizable gaits. The final resulting CPG dynamics for each gait, in terms of membrane potentials, are shown in Fig. 7. By thresholding the voltage traces, it is possible

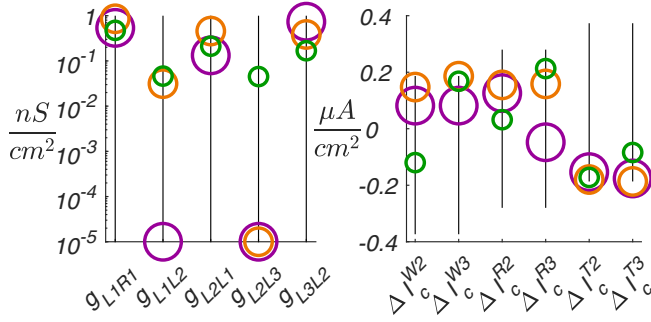


FIG. 6. Parameter sets x found by the PS optimization (orange circles), the GA optimization refined through pattern search (green circles), and the SO algorithm (purple circles). The black vertical lines indicate the range between the lower and the upper bounds constraining the explorable parameter space.

to distinguish between the swing phase (bursting activity of the corresponding cell) and stance phase (below-threshold activity of the corresponding cell), obtaining a representation of the three gaits, also shown in Fig. 7, that can be directly compared with the reference case of Fig. 5. The parameter values resulting from the optimization procedure and other model parameters are listed in Appendix C. All transitions between gaits, provoked by varying the control currents while leaving all other parameters unaltered, happen promptly and smoothly, as shown in Fig. 8 for the gaits obtained through particle swarm optimization.

The quantitative comparison between ideal and obtained phase lags is shown in Fig. 9, confirming the qualitative observation: in all cases, the obtained phase lags fall very close to their target values. In particular, PS optimization and GA-based optimization yielded ripple and tripod gaits that perfectly reproduce the ideal phase lags (maximum percent errors of 0.48% and 0.28% for the ripple gait, and 0.45% and 1.95% for the tripod gait, in the case of PS and GA, respectively); the wave gait presents slightly less accurate phase lags (maximum percent errors of 4.78% and 8.05% in the case of PS and GA, respectively). On the contrary, the surrogate optimization yielded a perfect wave gait (maximum percent error of 0.48%) and less accurate ripple and tripod gaits (maximum percent errors of 8.35% and 4.88%).

We also verify the adherence of the modeled gaits to the five rules of Wilson's system:

(1) Waves of forward leg movements do run from posterior to anterior and the overlap between the swing phases of ipsilateral legs, when present, is very small (maximum duration of 1.09%, 0.93%, and 3.28% of the step period for the wave gait and 0.41%, 0.53%, and 4.09% of the step period for the ripple gait in the case of PS, GA, and SO, respectively); there is no overlap between the swing phases of ipsilateral legs in any of the modeled tripod gaits.

(2) Contralateral legs are always in antiphase for all modeled gaits, with maximum overall errors of 0.22%, 0.87%, and 0.10% in the case of PS, GA, and SO, respectively.

(3) The mean duration of the swing phase, averaged over all legs and gaits, is 77.47 ms with a standard deviation of 13.43 ms for PS, 80.01 ms with a standard deviation of 4.08 ms for GA, and 73.26 ms with a standard deviation of 15.66 ms for SO [see also Fig. 10(a)]. This rule is thus

better fulfilled by the result obtained with the GA-based optimization.

(4) The duty cycle increases as the frequency increases, from wave, to ripple to tripod gait for all optimization algorithms, as shown in Fig. 11.

(5) The interval between adjacent ipsilateral legs, averaged over all leg pairs, is not constant across gaits; in particular, the interval grows significantly for the tripod gait for all optimization algorithms [see also Fig. 10(b)]. Thus this rule cannot be considered fulfilled in any case.

Overall, the modeled gait features appear in good agreement with Wilson's system, with only one of the five rules not fulfilled. We remark that, when defining the objective function for the parameter optimization of the hexapod CPG, we only imposed specific phase differences between limbs. Even if other gait features such as frequency, duty cycle, and duration of the swing phase were not codified in the objective function, the obtained model behavior is nonetheless compatible with these characteristics as they are observed in natural gaits. This finding corroborates the suitability of the obtained CPG model, in terms of both topology and neuron and synapse models.

VI. DISCUSSION AND CONCLUSIONS

Animal locomotion arises from the nontrivial interplay between the nervous system, the musculoskeletal system, and the environment, with multilayered and distributed control systems, with central networks, reflexes, and mechanics all contributing to sensorimotor responses on different timescales [35]. Because of this inherent complexity, it has been a longstanding challenge to understand (through integrative approaches involving biology, physics, engineering, and other disciplines) the structure, function, and integration of animal sensorimotor systems. In this paper, we focused on a part of the animal locomotion system, the CPGs, which provide a type of feedforward controller for locomotion that helps to overcome delays. CPGs are activated by descending driving signals and produce predetermined motor outputs for locomotion. The modulating *descending pathways* can activate selectively multiple interconnected modules of the CPG network that control the movement of each joint in each limb [4,36–38]. The adaptations achieved by sensory inputs can be fast, as when running in the forest, or slow, to accommodate the animal's growth. Such adaptations are typically mediated by short- and long-term forms of synaptic plasticity and can be induced by different cellular and synaptic mechanisms through actions at the network level [5].

As stated above, the animal locomotion system is highly complex and not completely understood in its mechanisms. In this paper, we proposed a possible strategy to derive functional models able to reproduce key features of the CPG component of this system. We proposed a method to set the parameters of interlimb multigait locomotion CPGs, based on the definition of an objective function that matches the network activity pattern to gait features. We considered networks with biologically accurate neuron and synapse models and minimalist topology, where gait switches are prompted by an input control current, while all other network parameters remain fixed. In this modeling framework, each CPG cell has a different

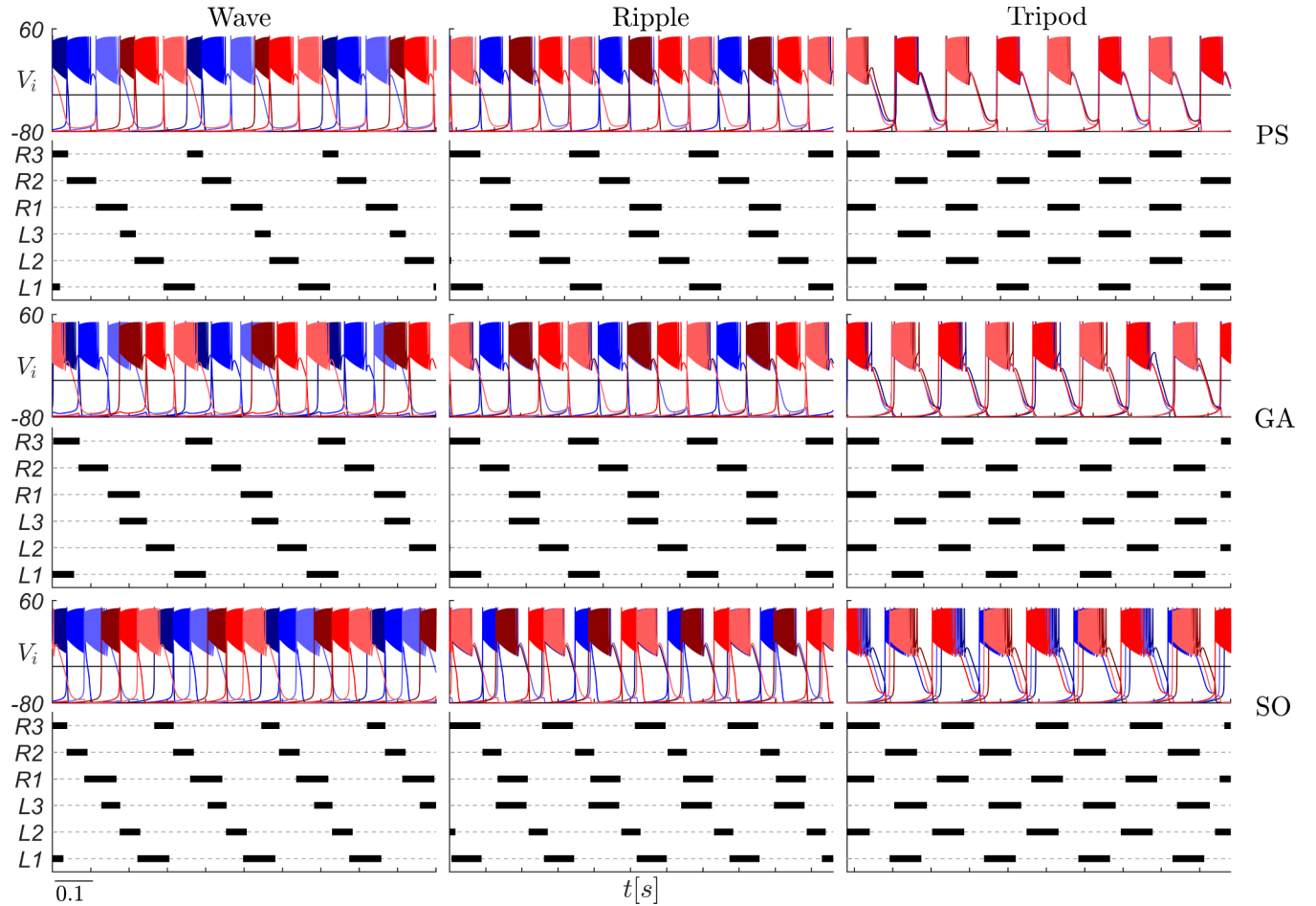


FIG. 7. Gaits obtained by simulating the hexapod CPG with the parameter sets x found by (from top to bottom) the CS, the PS optimization, the GA optimization refined through pattern search, and the SO algorithm. Color coding as in Fig. 4. The three gaits are also represented by thresholding the voltage traces: black bars correspond to the swing phases, and blank spaces represent the stance phases of each leg. Wave was obtained for $I_c^W = -0.057 \frac{\mu\text{A}}{\text{cm}^2}$ ($I_c^W = -0.059 \frac{\mu\text{A}}{\text{cm}^2}$ for the GA optimization), ripple for $I_c^R = -0.15 \frac{\mu\text{A}}{\text{cm}^2}$, and tripod for $I_c^T = -0.243 \frac{\mu\text{A}}{\text{cm}^2}$.

input control current (I_c^G for the reference cell, $I_c^G + \Delta I_c^{G_i}$ for the others). Therefore, even if the network topology is fixed and simple and we do not have interconnected modules that are activated or deactivated by the descending pathways, each CPG cell has its own “descending modulation”. In other words, we have proposed a functional model that captures some key features of the system owing to complex dynamics and simple topology. Of course, the same relevant features may be captured by adopting a complementary approach, with simpler dynamics and more complex topology. The main strength of our approach is that it allows accounting for the short-term synaptic modulation, which is likely at the basis of gait switching. Despite the high level of abstraction of our functional circuits, we obtained plausible gait transitions. Our modeling strategy could be a useful tool to obtain crucial comparative insights in the comparison of the locomotion systems of animals with different complexity levels [35] or at different growth stages [37].

We explored the use of derivative-free global optimization algorithms for the minimization of the proposed objective function. Global optimization has already been shown to effectively identify parameters for biologically detailed neuron

models [39]. We remark that, by contrast with many other works on CPG parameter setting, here we do not focus on retracing experimentally observed membrane potential profiles or reproducing elicited firing rates, but on matching high-level network dynamics characteristics to target gaits. We first tested three global optimization algorithms on an existing multigait quadruped CPG network, reaching the double objective of (1) validating the effectiveness of the previously proposed parameter setting custom strategy [14,18] and (2) testing the suitability of the proposed objective function for reaching accurate modeling of quadruped gaits, independently from the chosen global optimization algorithm.

The obtained results could be extended to quadrupeds other than mice (with different biomechanical characteristics) by using as reference the experimental data in [40] or similar papers.

We then introduced a novel multigate interlimb hexapod CPG model based on the principle of maintaining a fixed network structure and prompting gait switches through a variable control current. Exploiting the proposed method for tuning the model parameters, we were able to accurately model the three main hexapod gaits and the transitions between them,

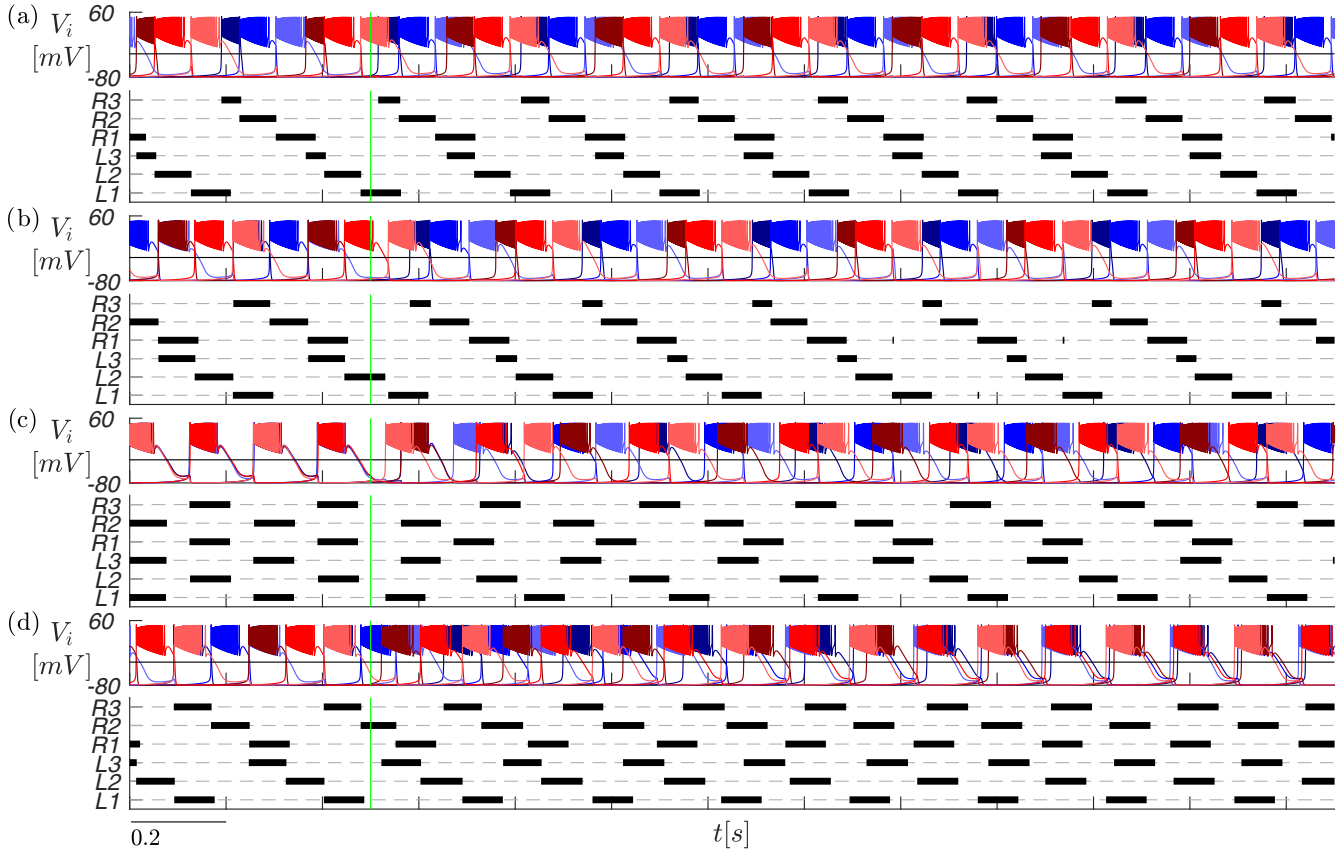


FIG. 8. Membrane potential traces of the CPG neurons (upper plots with colored traces) and corresponding swing and stance phases representation (swing phase in black) for all gait transitions: (a) wave to ripple, (b) ripple to wave, (c) tripod to ripple, and (d) ripple to tripod. The change in control currents that prompts the gait transition is marked by the green vertical line.

with all the tested global optimization algorithms. In particular, we directly obtained suitable parameter sets when using PS optimization and SO, while we refined the less accurate results from the GA using local pattern search optimization and carrying out a second optimization round focusing on the wave gait.

We observe that the conductances of the inhibitory synapses connecting the contralateral CPG cells have the strongest overall values in the case of the PS optimization and the GA optimization and the second strongest value in the case of the SO, underlying their key role in maintaining anti-phase

coordination between contralateral legs during all exhibited gaits. Additionally, we observe that the values of the synaptic conductances obtained through our method with all global optimization algorithms (see Appendix C) display anterior-to-posterior inhibitory connections (g_{L2L1} , g_{L3L2} and equivalents on the right side) much stronger than the posterior-to-anterior ones (g_{L1L2} , g_{L2L3} and equivalents on the right side).

In this work, we used specific neuron and synapse models that enable controlling phase differences, frequency, and duty cycle compatibly with gait modeling, by modifying only the control current. The characteristics of these models are

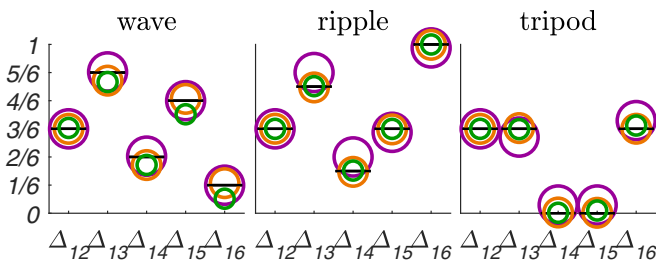


FIG. 9. Representation of the ideal (black bars) and obtained (colored circles) phase differences between limbs for the wave, ripple, and tripod gaits. Color code as follows: orange circles for PS optimization, green circles for the GA optimization refined through pattern search, and purple circles for the SO algorithm.

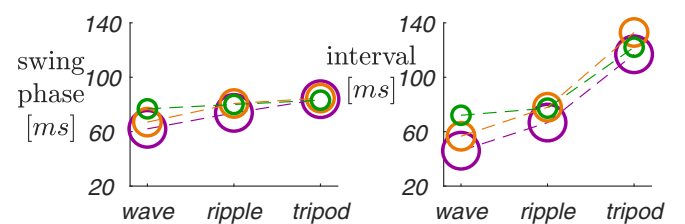


FIG. 10. (a) Duration of the swing phase and (b) interval between adjacent ipsilateral legs for wave, ripple, and tripod gaits. Colored circles mark the average value among (a) the six CPG cells or among (b) the four ipsilateral leg pairs. Color code as follows: orange circles for PS optimization, green circles for the GA optimization refined through pattern search, and purple circles for the SO algorithm.

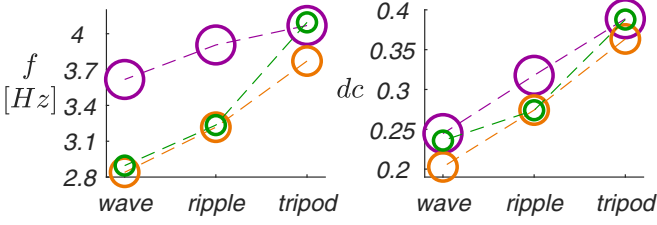


FIG. 11. Frequency f and duty cycle dc values for wave, ripple, and tripod gaits. Colored circles mark the average value among the six CPG cells. Color code as follows: orange circles for PS optimization, green circles for the GA optimization refined through pattern search, and purple circles for the SO algorithm.

especially relevant when designing multigait CPGs that are required to reproduce gaits with different phase lags between corresponding contralateral legs, such as the quadruped CPG, as explained in detail in [17,18]. We maintained the same models for the proposed hexapod CPG, omitting the excitatory synapses, since hexapod terrestrial gaits only exhibit contralateral legs in antiphase. Regardless, the proposed parameter setting approach, consisting of defining an objective function based on the adherence of the CPG's emergent dynamics to the target gait features, remains valid independent of the neuron and synapse models, number of legs, and parameters to be optimized.

ACKNOWLEDGMENT

The authors would like to thank their colleague and friend Andrey Shilnikov for his role in developing the CPG modeling strategy.

APPENDIX A: THALAMIC RETICULAR NEURON MODEL

The thalamic reticular neuron model [19,20] is defined by the following state equations:

$$\begin{aligned} \xi \frac{dV}{dt} &= \frac{-I_T - I_L - I_{Na} - I_K - I_c + I^{syn}}{C}, \\ \xi \frac{dCa}{dt} &= -\frac{kI_T}{2FD} - \frac{K_T Ca}{Ca + K_d}, \\ \xi \frac{dy}{dt} &= \frac{y^\infty - y}{\tau_y}, \quad y \in \{h, m, n, m_T, h_T\}, \end{aligned} \quad (A1)$$

where V is the membrane potential of the neuron, Ca is the intracellular calcium concentration, and y stands for the generic gating variable. The vector \mathbf{y} in Eq. (1) is thus defined as $\mathbf{y} = [Ca, h, m, n, m_T, h_T]$. The only difference with respect to the original model is the presence of the dimensionless coefficient ξ , which scales the time variable t and thus regulates the burst frequency f so that it spans the range required to model the desired gaits. The ion currents I_T (calcium), I_{Na} (sodium), I_K (potassium), and I_L (leakage) evolve according to the following equations:

$$\begin{aligned} I_T &= g_{Ca} m_T^2 h_T (V - E_{Ca}), \quad I_L = g_L (V - E_L), \\ I_{Na} &= g_{Na} m^3 h (V - E_{Na}), \quad I_K = g_K n^4 (V - E_K), \end{aligned}$$

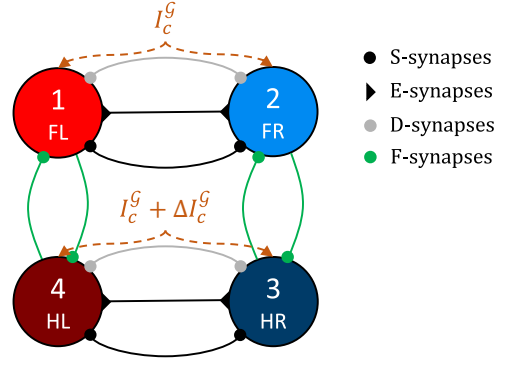


FIG. 12. CPG circuit of four coupled cells labeled as follows: FL or FR, fore-left or right, and HL or HR, hind-left or right. The symbols \blacktriangleright , \bullet , \circ , and \circ denote, respectively, the excitatory E and inhibitory S , F , and D synapses (see Table IV). Each CPG cell controls flexor muscles regulating the swing phase of a limb, and D synapses simulate the actions of the neural populations (not explicitly represented in the given model) controlling the extensor muscles. The fore and hind gHCOs are coupled through ipsilateral F synapses.

which depend on V and on the gating variables h (inactivation variable of the Na^+ current), m (activation variable of the Na^+ current), n (activation variable of the K^+ current), m_T (activation variable of the low-threshold Ca^{2+} current), h_T (inactivation variable of the low-threshold Ca^{2+} current). All gating variables evolve according to the differential equations written above for y , where

$$\begin{aligned} y^\infty &= a_y / (a_y + b_y), \quad \tau_y = 1 / (a_y + b_y) \quad (y = \{h, m, n\}), \\ a_h &= 0.128 e^{\frac{17-V}{18}}, \quad b_h = \frac{4}{e^{-0.2(V-40)} + 1}, \\ a_m &= \frac{0.32(13-V)}{e^{0.25(13-V)} - 1}, \quad b_m = \frac{0.28(V-40)}{e^{0.2(V-40)} - 1}, \\ a_n &= \frac{0.032(15-V)}{e^{0.2(15-V)} - 1}, \quad b_n = 0.5 e^{\frac{10-V}{40}}, \\ m_T^\infty &= \frac{1}{1 + e^{\frac{V+52}{7.4}}}, \quad \tau_{mT} = 0.44 + \frac{0.15}{e^{\frac{V+27}{10}} + e^{-\frac{V+102}{15}}}, \\ h_T^\infty &= \frac{1}{1 + e^{\frac{V+80}{5}}}, \quad \tau_{hT} = 62.7 + \frac{0.27}{e^{\frac{V+48}{4}} + e^{-\frac{V+407}{50}}}. \end{aligned}$$

In the above equations, the leakage current I_L has conductance $g_L = 0.05 [\frac{mS}{cm^2}]$ and reversal potential $E_L = -78 [mV]$; I_{Na} and I_K are the fast Na^+ and K^+ currents responsible for the generation of action potentials, with conductances $g_{Na} = 100 [\frac{mS}{cm^2}]$ and $g_K = 10 [\frac{mS}{cm^2}]$ and reversal potentials $E_{Na} = 50 [mV]$ and $E_K = -95 [mV]$; I_T is the low-threshold Ca^{2+} current that mediates the rebound burst response, with

TABLE IV. Synapse types.

Synapse type	Abbreviation	Symbol
Fast excitatory	E	\blacktriangleright
Slow inhibitory	S	\bullet
Delayed fast inhibitory	D	\circ
Fast inhibitory	F	\circ

TABLE V. Parameter values obtained with the CS and with the global optimization algorithms: PS, GA, SO.

Parameter	CS	PS	GA	SO
g_{12}^S	0.1207	0.1208	0.1208	0.1203
g_{12}^E	0.0052	0.0052	0.0052	0.0052
g_{41}^F	0.0048	0.0047	0.0048	0.0062
g_{14}^F	0.0111	0.0111	0.0108	0.0111
g_{12}^D	0.0118	0.0117	0.0118	0.0134
ΔI_c^W	-0.0571	-0.0569	-0.0549	-0.0572
ΔI_c^T	0.0343	0.0339	0.0560	0.0344
ΔI_c^B	0.0571	0.0579	0.0693	0.0570

conductance $g_{Ca} = 1.75 [\frac{mS}{cm^2}]$ and reversal potential $E_{Ca} = k_0 \frac{RT}{2F} \log(\frac{Ca_0}{Ca})$; I^{syn} is the synaptic current; see Eq. (2). When the control current I_c is in the range $[-0.43, 0.13] [\frac{\mu A}{cm^2}]$ the neuron exhibits bursting behavior. The other parameters are set as follows: $C = 1 [\frac{\mu F}{cm^2}]$, $Ca_0 = 2 [mM]$, $D = 1 [\mu m]$, $K_T = 0.0001 [mM ms]$, $K_d = 0.0001 [mM]$, $F = 96.489 [\frac{C}{mol}]$ is the Faraday constant, $R = 8.31441 [\frac{J}{mol K}]$ is the universal gas constant, and the temperature T is set at $309.15 [K]$.

APPENDIX B: QUADRUPEL CPG MODEL AND PARAMETER VALUES

The quadruped CPG network from [18] is displayed in Fig. 12. In this case, the term I_i^{syn} groups together the synaptic currents from four different synapse types, listed in Table IV:

$$I_i^{syn} = \sum_{j=1}^4 \{g_{ij}^E[E^E - V_i(t)]s_j^E + g_{ij}^S[E^S - V_i(t)]s_j^S + g_{ij}^D[E^S - V_i(t - \delta)]s_j^D + g_{ij}^F[E^S - V_i(t)]s_j^F\}. \quad (B1)$$

TABLE VI. Top: parameter values obtained with all global optimization algorithms. Bottom: other synapse parameters as in [17].

Parameter	PS	GA (+Psearch)	SO
g_{L1R1}	0.8551	0.4741	0.5380
g_{L1L2}	0.0314	0.0461	10^{-5}
g_{L2L1}	0.4573	0.2117	0.1328
g_{L2L3}	10^{-5}	0.0451	10^{-5}
g_{L3L2}	0.3845	0.1679	0.7370
ΔI_c^{W2}	0.1474	-0.1199	0.0818
ΔI_c^{W3}	0.1860	0.1680	0.0818
ΔI_c^{R2}	0.1551	0.0320	0.1260
ΔI_c^{R3}	0.1586	0.2129	-0.0479
ΔI_c^{T2}	-0.1798	-0.1723	-0.1536
ΔI_c^{T3}	-0.1865	-0.0841	-0.1760
α		0.7543	
β		0.0391	
θ		17.500	
ν		10	
E		60	

Slow S synapses are modeled by the first-order kinetic model, while other synapse types are modeled using the FTM approach.

The parameter values obtained with the custom optimization strategy and with the global optimization algorithms are listed in Table V. All other parameters are set as in [18].

APPENDIX C: HEXAPOD CPG PARAMETER VALUES

The parameter values obtained with all global optimization algorithms are listed in the top part of Table VI (above the horizontal line). The other synapse parameters are set as in the bottom part of the table (below the horizontal line) and taken from [17].

- [1] E. Marder and D. Bucher, *Curr. Biol.* **11**, R986 (2001).
- [2] A. J. Ijspeert, *Neural Netw.* **21**, 642 (2008).
- [3] S. L. Hooper and B. Ansgar (Eds.), *Neurobiology of Motor Control: Fundamental Concepts and New Directions* (John Wiley & Sons, Hoboken, NJ, 2017), pp. 225–262.
- [4] O. Kiehn and K. Dougherty, in *Neuroscience in the 21st Century: From Basic to Clinical*, edited by D. W. Pfaff, N. D. Volkow, and J. L. Rubenstein, 3rd ed. (Springer, Cham, Switzerland, 2022), pp. 1623–1652.
- [5] S. Grillner, *Neuron* **52**, 751 (2006).
- [6] K. Takakusaki, *Movement Disorders* **28**, 1483 (2013).
- [7] V. Caggiano, R. Leiras, H. Goñi-Erro, D. Masini, C. Bellardita, J. Bouvier, V. Caldeira, G. Fisone, and O. Kiehn, *Nature (London)* **553**, 455 (2018).
- [8] P. A. Guertin, *Brain Res. Rev.* **62**, 45 (2009).
- [9] P. A. Guertin, *Front. Neurol.* **3**, 183 (2013).
- [10] C. Mantziaris, T. Bockemühl, and A. Büschges, *Dev. Neurobiol.* **80**, 16 (2020).
- [11] R. M. Ghigliazza and P. Holmes, *SIAM J. Appl. Dyn. Syst.* **3**, 671 (2004).
- [12] S. Fujiki, S. Aoi, T. Funato, N. Tomita, K. Senda, and K. Tsuchiya, *Phys. Rev. E* **88**, 012717 (2013).
- [13] S. M. Danner, S. D. Wilshin, N. A. Shevtsova, and I. A. Rybak, *J. Physiol.* **594**, 6947 (2016).
- [14] M. Lodi, A. L. Shilnikov, and M. Storace, *IEEE Trans. Neural Netw. Learn. Syst.* **31**, 3658 (2020).
- [15] J. Yu, M. Tan, J. Chen, and J. Zhang, *IEEE Trans. Neural Netw. Learn. Syst.* **25**, 441 (2013).
- [16] P. Ramdya and A. J. Ijspeert, *Sci. Robot.* **8**, eadg0279 (2023).
- [17] V. Baruzzi, M. Lodi, M. Storace, and A. Shilnikov, *Phys. Rev. E* **102**, 032406 (2020).
- [18] V. Baruzzi, M. Lodi, M. Storace, and A. Shilnikov, *Phys. Rev. E* **104**, 064405 (2021).
- [19] A. Destexhe, D. Contreras, T. J. Sejnowski, and M. Steriade, *J. Neurophysiol.* **72**, 803 (1994).

- [20] R. Nagornov, G. Osipov, M. Komarov, A. Pikovsky, and A. Shilnikov, *Commun. Nonlinear Sci.* **36**, 175 (2016).
- [21] X.-J. Wang and J. Rinzel, *Neural Comput.* **4**, 84 (1992).
- [22] D. Somers and N. Kopell, *Biol. Cybern.* **68**, 393 (1993).
- [23] X.-J. Wang, *Neuroscience* **89**, 347 (1999).
- [24] D. V. Buonomano, *J. Neurosci.* **20**, 1129 (2000).
- [25] S. Jalil, I. Belykh, and A. Shilnikov, *Phys. Rev. E* **85**, 036214 (2012).
- [26] J. Kennedy and R. Eberhart, in *Proceedings of ICNN'95—International Conference on Neural Networks, Perth, WA, Australia*, Vol. 4 (IEEE, 1995), pp. 1942–1948.
- [27] J. H. Holland, *Sci. Am.* **267**, 66 (1992).
- [28] H.-M. Gutmann, *J. Global Optim.* **19**, 201 (2001).
- [29] C. Bellardita and O. Kiehn, *Curr. Biol.* **25**, 1426 (2015).
- [30] M. Lemieux, N. Josset, M. Roussel, S. Couraud, and F. Bretzner, *Front. Neurosci.* **10**, 42 (2016).
- [31] M. Lodi, A. Shilnikov, and M. Storace, CEPAGE: A toolbox for Central Pattern Generator analysis, in *Proceedings of the 2017 IEEE International Symposium on Circuits and Systems (ISCAS'2017)* (IEEE, 2017), pp. 1266–1269.
- [32] R. Barrio, Á. Lozano, M. Martínez, M. Rodríguez, and S. Serrano, *Neurocomputing* **461**, 679 (2021).
- [33] D. M. Wilson, *Annu. Rev. Entomol.* **11**, 103 (1966).
- [34] J. A. Nirody, *Integ. Compar. Biol.* **61**, 710 (2021).
- [35] A. J. Ijspeert and M. A. Daley, *J. Exp. Biol.* **226**, jeb245784 (2023).
- [36] M. Goulding, *Nat. Rev. Neurosci.* **10**, 507 (2009).
- [37] O. Kiehn, *Curr. Opin. Neurobiol.* **21**, 100 (2011).
- [38] O. Kiehn, *Nat. Rev. Neurosci.* **17**, 224 (2016).
- [39] N. W. Gouwens, J. Berg, D. Feng, S. A. Sorensen, H. Zeng, M. J. Hawrylycz, C. Koch, and A. Arkhipov, *Nat. Commun.* **9**, 710 (2018).
- [40] L. Maes and A. Abourachid, *J. Exp. Biol.* **216**, 2257 (2013).